A numerical study of reflectometer performance

Michelsen, P.; Pécseli, H.L.

Publication date:
1991

Document Version
Publisher's PDF, also known as Version of record

RISØ

Risø-R-592(EN)

A Numerical Study of Reflectometer Performance

Poul Michelsen and Hans Pécseli

Risø National Laboratory, Roskilde, Denmark
December 1991

Risø–R–592(EN)

A Numerical Study of Reflectometer Performance

Poul Michelsen and Hans Pécseli

Risø National Laboratory, Roskilde, Denmark
December 1991

Abstract In this report some basic features of the performance of a two frequency reflectometer used as a diagnostic for random plasma fluctuations are studied. Using a realistic and tractable model for the plasma fluctuations we derived some analytical results for correlation and crosscorrelation functions for the temporally varying phase of the reflected signals. Numerical simulations were performed to illustrate the practical applicability of the basic ideas of the reflectometer. The studies were carried out mainly for incoming electromagnetic waves in ordinary polarization.

ISBN 87-550-1748-7
ISSN 0106-2840

Grafisk Service · Risø · 1991

Contents

1 Introduction

In tokamaks and other types of plasma experiments, a diagnostic to measure plasma density fluctuations is important in order to obtain an understanding of plasma turbulence and plasma transport. A measuring technique denoted reflectometry has been used for some years in tokamak experiments in order to measure density profiles and their motion (see e. g.: Cavallo and Cano, 1982, Simonet, 1985, or Sips, 1991). In a way the method is based on the same ideas as an ionosonde, which is used for measuring the plasma density in the lower part of the ionosphere. When a microwave beam is launched against the plasma surface it is reflected at the position where the frequency is equal to the plasma cut-off frequency. By measuring the phase change of the reflected wave it is possible to follow movements of the plasma surface. With a fixed-frequency oscillator only a single density point can be monitored, while it is necessary to use a multi-frequency system in order to detect simultaneously the entire density profile. In order to interpret the results, the phase change of the wave is normally calculated according to the approximation of geometrical optics, often called the WKB approximation. If the phase change is measured for all frequencies, the density profile can be calculated from an Abel conversion assuming the WKB approximation. In most cases the wavelength of the microwave is short compared to typical plasma density gradient length and the approximation is rather good.

Recently the principles of a new technique for diagnosing microturbulence called correlation reflectometry was presented (Costley and Cripwell, 1989, and Cripwell and Costley 1991). Two microwave beams with a small difference in frequency are launched against the density profile. The two phases can be measured versus time and since these phases are functions of plasma cut-off layer positions, it is possible by a crosscorrelation technique to detect the relative motion of plasma perturbations between two different positions. By using a variety of frequency differences between the two microwave beams it has been possible (Costley and Cripwell, 1989) to obtain a full dispersion curve for the plasma waves giving essential information about the plasma turbulence.

In a plasma where the turbulence has characteristic scale lengths smaller than or of the same order as the microwave wavelength, it is questionable if an analysis of the measurements from correlation reflectometry based on the WKB approximation will lead to the correct conclusions. To investigate this question we have solved the wave equation with a new numerical procedure, which can solve a system of differential equations as a boundary value problem.

Statistical information on density fluctuation turbulence in tokamaks (and perhaps other plasmas) may in principle be obtained from a two-frequency reflectometer. However, the interpretation of the signals is difficult. An analysis based on an analytic treatment of the wave equation has recently been published by Zou et al., 1991. This analysis requires several assumptions to be satisfied. The main assumptions are that the characteristic length and time scale of the fluctuations must be less than that of the unperturbed plasma, since a local Fourier transform is applied, and that the turbulence level has to be low enough so the fluctuations can be treated as a perturbation in the wave equation. An analysis without such basic assumptions is only possible from a numerical calculation.

We carry out a performance study of a model of a two-frequency reflectometer. A level of random plasma density fluctuations is modelled in plane geometry by superimposing moving density pulses on a given density profile. By the proper choice of the shapes of these pulses, we are in principle able to model any spectrum for disturbances propagating in the direction along the density gradient. With the speed of propagation known in the numerical experiment, we are able to determine

the accuracy of the predictions of the characteristic velocity deduced from the crosscorrelation of the fluctuating phase signals of the reflectometer. Studies are carried out for statistically distributed disturbance velocities and for varying levels of a superimposed small-scale random noise component. The analysis uses the the fullwave solution discussed above, but the accuracy of a somewhat simpler WKB solution is tested also.

In Sec. 2 the WKB approximation and its limitations are discussed briefly. Section 3 gives the wave equation and derives the appropriate boundary conditions, and some numerical results are presented in Sec. 4. In Sec. 5. a discussion of the plasma model and the correlation analysis can be found. Section 6 introduces a new data analysis method called coincidence counting, which in some cases may extract more information out of the measurements than the usual correlation technique. Finally, discussions and conclusions are given in Sec. 7

2 The WKB approximation

An electromagnetic wave injected into a plasma perpendicular to the magnetic field may be reflected at a cut-off layer. For an ordinary wave (E-field parallel to magnetic field) the cut-off frequency is: $\omega = \omega_{pe} = \sqrt{e^2 n_0/\epsilon_0 m}$, and for an extraordinary wave the cut-off frequency is: $\omega = \sqrt{\omega_{pe}^2 + \omega_{ce}^2}$, where $\omega_{ce} = eB_0/m$. An approximation for the phase of the reflected wave with respect to the phase of the incoming wave is given in the book by Ginzburg. 1964:

$$\varphi_1(\omega) = \frac{2\omega}{c}\int_0^R N(x,\omega)dx - \frac{\pi}{2} \tag{1}$$

where N is the refractive index, x the position co-ordinate, ω the cyclic wave frequency and R is the reflection point. The expression is exact if the plasma density has a linear density variation. In this case the solution to the wave equation can be expressed in terms of Airy functions. Since the integral term is the normal approximation of geometrical optics often called the WKB approximation, valid if the wavelength is small compared to the characteristic gradient length, we can interpret the $-\pi/2$ term as the phase jump at the reflection layer. If the refractive index has a linear dependence in an interval around the reflection point of the order of some wavelengths we can therefore expect the expression (1) to be a good approximation for the total phase shift. The correct condition for the WKB approximation to be satisfied is according to Ginzburg. 1964:

$$\frac{\lambda_0}{2\pi}\frac{|\frac{dN}{dx}|}{|N^2|} \ll 1 \tag{2}$$

where λ_0 is the vacuum wavelength and x is the space co-ordinate. The inequality shows that the WKB approximation breaks down if the diffractive index is too small or if the derivative of the diffractive index is large. This means that the approximation always breaks down close to the reflection point, i.e.: the phase calculated from (1) will always be uncertain due to this fact. On the other hand it is worth noting the 2π factor which shows that the correct parameter to be compared to the gradient length is $\lambda/2\pi$. This is rather significant since the errors which may occur by using the approximation can be shown to decrease exponentially with this factor (Ginzburg, 1964).

To get a more precise idea of how close to the reflection point the approximation can be used let us consider a specific case. We shall consider a plasma with a linear increasing density according to the expression: $n = n_0 x/m\lambda_0$, where n_0 is the critical density and m the number of vacuum wavelength from the plasma edge to

the reflection point. The refractive index for an ordinary wave is $N = \sqrt{1 - n/n_0}$. The condition (2) will then be

$$\frac{\Delta x}{\lambda_0} \gg \frac{m^{1/3}}{(4\pi)^{2/3}} \simeq 0.19 m^{1/3}. \tag{3}$$

where Δx is the minimum distance from the reflection point where condition (2) is satisfied. From this we can see that for a steep density profile ($m \simeq 1$) the uncertainty using (1) may be of the order of λ_0, and for very gentle density gradients ($m \simeq 100$), it is of the order of a few λ_0. For reflection of the extraordinary wave the profile of refractive index is typical more flat which means that the approximation leads to a larger uncertainty in determination of the point of reflection.

3 The full wave solution

3.1 The wave equation

We consider electromagnetic waves propagating in the x-direction in a plasma with an inhomogeneous density $n(x)$ in a constant magnetic field $B_o\hat{z}$. The wave equation can be written as:

$$\frac{d^2E}{d\xi^2} = -\epsilon(\xi)E, \tag{4}$$

where $\xi = xk_0$ with k_0 the wavenumber in free space. We have for the O-mode that $E = E_z$ and $\epsilon = \epsilon_{zz}$ and for the X-mode that $E = E_y$ and $\epsilon = \epsilon_{xx} + \epsilon_{xy}^2/\epsilon_{xx}$. Here the components of the dielectric tensor are

$$\epsilon_{xx} = 1 - \frac{X(1+iZ)}{(1+iZ)^2 - Y^2}, \quad \epsilon_{xy} = i\frac{XY}{(1+iZ)^2 - Y^2}, \quad \epsilon_{zz} = 1 - \frac{X}{1+iZ} \tag{5}$$

The normalized density X, the normalized magnetic field Y, and the normalized collision frequency Z are defined by

$$X = \frac{\omega_{pe}^2}{\omega^2}, \quad Y = \frac{\omega_{ce}}{\omega}, \quad Z = \frac{\nu}{\omega}, \tag{6}$$

where $\omega_{pe}(\xi) = (n(\xi)e^2/\epsilon_0 m)^{\frac{1}{2}}$ and $\omega_{ce}(\xi) = eB(\xi)/m$ are the electron plasma frequency and the gyro-frequency, respectively.

3.2 The boundary conditions

To solve the equation (4) we have to specify the necessary boundary conditions. Assume the inhomogeneous part of the plasma is surrounded by a homogeneous plasma i.e.: $n = n_0$ for $\xi \leq 0$ and $n = n_1$ for $\xi \geq a$. In the homogeneous plasma ranges the wave solution is the solution to eq.(4) with constant ϵ:

$$E(\xi) = c_1 \exp(iN_x\xi) + c_2 \exp(-iN_x\xi) \tag{7}$$

where N_x is the x-component of the refractive index. The matching condition at the border between the homogeneous and the inhomogeneous plasma is determined by that the E-field and the derivative of the E-field (really the B-field) must be continuous across the boundary. At the left boundary we let the incoming wave have the amplitude $c_1 = 1$. If the E-field at the boundary is E_0 the boundary condition can be written as:

$$iN_xE_0 + E_0' = 2iN_x \tag{8}$$

where E_0' is the derivative of $E(\xi)$ at $\xi = 0$ and the constant c_2 is given by

$$c_2 = (E_0 - 1) \tag{9}$$

At the right boundary, $\xi = a$ there will be no left-going wave, i.e.: $c_2 = 0$, which gives the boundary condition:

$$iN_x E_a - E'_a = 0 \tag{10}$$

where E'_a is the derivative of $E(\xi)$ at $\xi = a$ and $c_1 = E_a \exp(-iN_x a)$. This means that the wave solution for $\xi \leq 0$ is:

$$E = \exp(iN_x\xi) + (E_0 - 1)\exp(-iN_x\xi). \tag{11}$$

and for $\xi \geq a$ we get:

$$E = E_a \exp[iN_x(\xi - a)] \tag{12}$$

where E_0 and E_a are the E-fields at the left and right boundary, respectively

4 Numerical solutions

The full wave equation (4) with the boundary conditions (8) and (10) was solved by use of the numerical code COLSYS by Ascher, Christiansen and Russel, 1979. This code can solve boundary-value problems for mixed-order systems of ordinary differential equations. The solution method is based on spline collocation, and the code automatically finds an appropriate distribution of mesh points in order to keep the local error within certain limits specified by the user.

A similar but more general system of equations taking into account oblique propagation with respect to the magnetic field solved by COLSYS was treated by Hansen et al., 1988a, in order to investigate wave conversion.

In Fig. 1a the wave solution for an ordinary wave propagating against a steep density gradient is shown. The density is zero at the left boundary and it is equal to twice the critical density at the right boundary. In Fig. 1b corresponding curves for a wave in a density distribution with a smooth gradient are shown. A WKB

Figure 1. Wave solution for an ordinary wave reflected at the cut-off position and the density profile. a) a plasma with a steep density gradient, b) a plasma with a smooth density gradient.

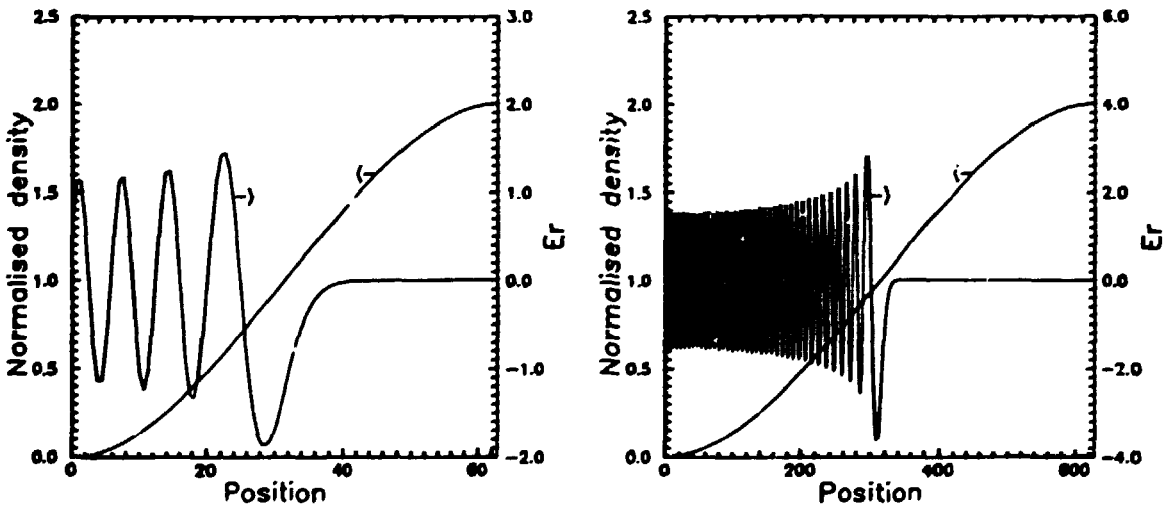

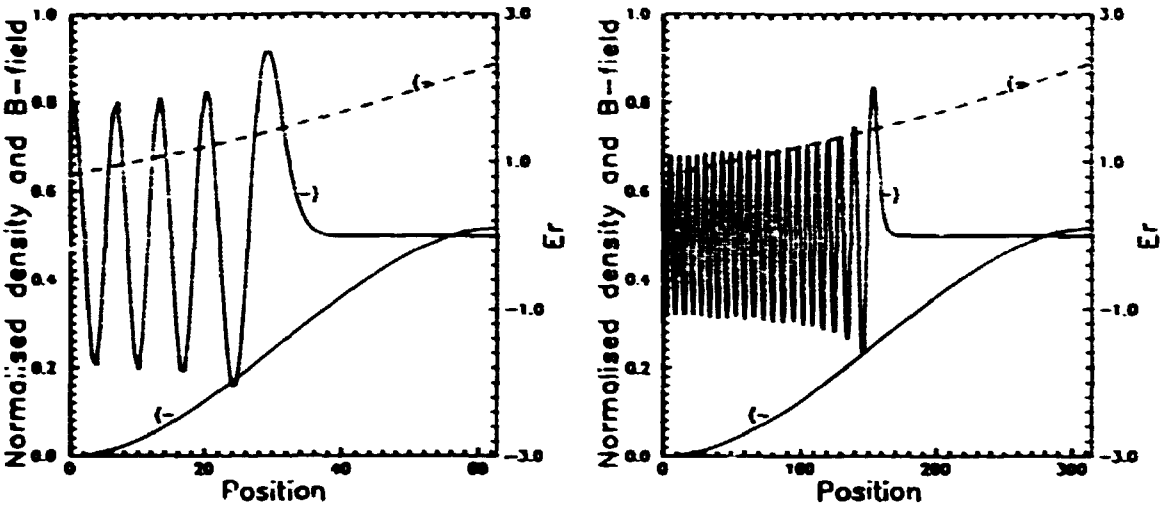

Figure 2. Wave solution for an extra-ordinary wave reflected at the cut-off position. a) a plasma with a steep density gradient, b) a plasma with a smooth density gradient. The variation of the magnetic field is shown by the dashed lines.

solution will in this case give nearly the same solution. Corresponding results for extra-ordinary polarization are shown in Fig. 2a and 2b. This polarization was used by Cripwell and Costley 1991.

In order to see how a small narrow pulse will influence on the reflected wave Fig. 3 shows a model with a pulse moving along a smooth density gradient. The pulse half-width is in this case equal to five wavelengths and has an amplitude equal to 0.2 times the critical density. In Fig. 4a the phase of the reflected wave at the left boundary is shown as a function of time, calculated by COLSYS (solid line) and by a WKB approximation according to formula (1) (dashed line). Similar curves are shown in Fig. 4b with a more narrow pulse with a half-width equal to one wavelength and of the same amplitude as in Fig. 3. It is seen here that large differences in the wave-field will appear when a density pulse with a width comparable to the wavelength moves in a standing wave.

5 Reflectometry modelling

5.1 The plasma model

In our numerical model the exact phase information from the reflected waves can be obtained without some of the problems which occur in a real experiment e.g. wave scattering in various directions. These problems are treated in several of the experimental papers and are not considered here.

The objective of this work is to investigate what is the maximum amount of information about the statistics of the plasma turbulence that we can obtain from a perfect correlation reflectometer. With our full-wave calculation we only have to introduce two assumptions concerning the plasma motion and density profile. The first is that we assume that plasma motion is slow compared to the speed of the electromagnetic modes, and therefore, we can calculate the wave pattern and

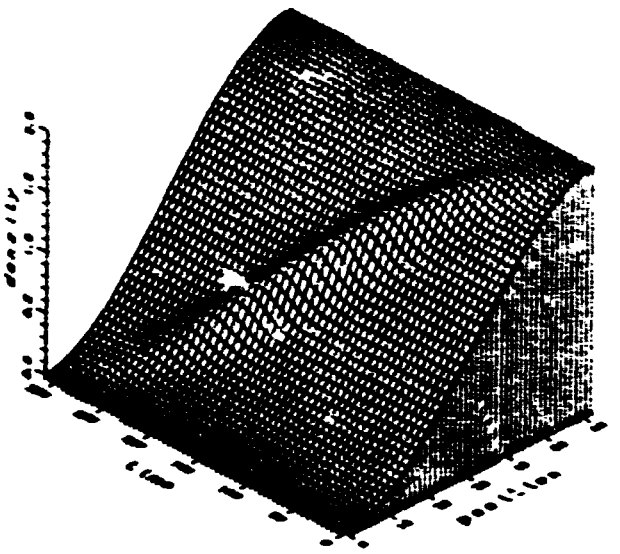

Figure 3. A pulse moving along a density gradient.

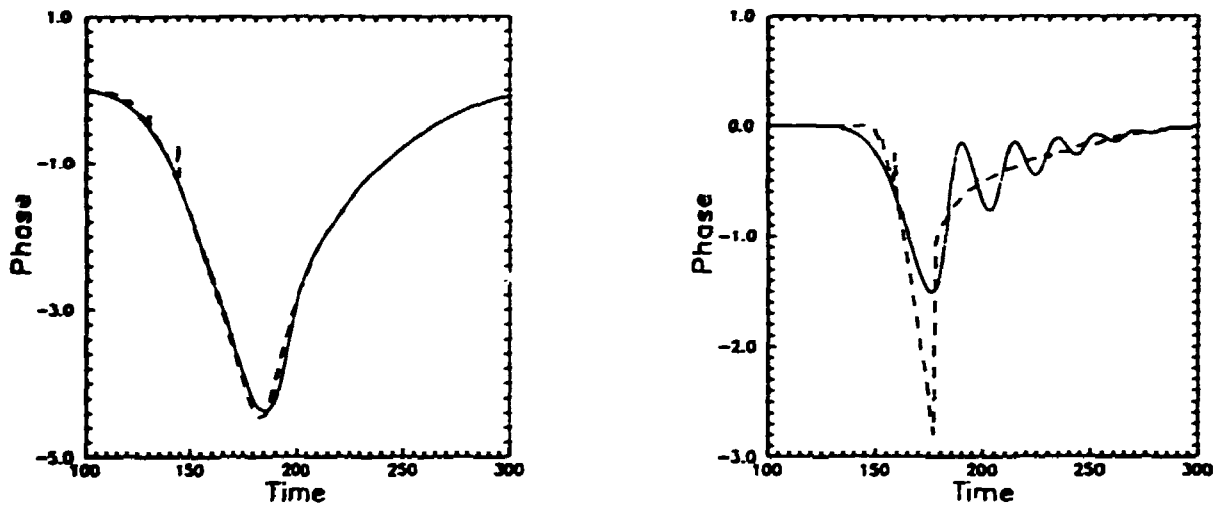

Figure 4. Phase of reflected wave versus time when a pulse is moving along the density gradient. Solid line is full wave solution, and dashed line is WKB solution. a) The half-width of the pulse is five wavelength, b) The half-width of the pulse is one wavelength.

thereby the phase of the reflected wave for a stationary plasma profile neglecting plasma motion. The other assumption described in Sec. 3.2 is necessary in order to have well defined boundary conditions. This requires that the one-dimensional plasma is surrounded by regions of constant density. The plasma density profile is separated into three parts. The stationary background density is given by:

$$n(\xi) = n_0\xi^2(3 - 2\xi) \tag{13}$$

which is the lowest order polynomial with zero slope at $\xi = 0$ and at $\xi = 1$, and which is equal to 0 at $\xi = 0$ and equal to n_0 at $\xi = 1$. On top of the stationary density profile a noisy background is superimposed. The noise is generated by superimposing a large number of bell-shaped pulses with random positive or negative amplitudes within a certain range, with given width, and with a random velocity direction.

As the simplest model we describe the fluctuations in plasma density as composed of a linear superposition of pulses having constant shapes and propagating with constant velocity. The pulses may have M different shapes labelled by the index ℓ. One such pulse gives rise to a certain phase variation $\phi_\ell(t - t_{j,\ell})$ of the electromagnetic wave as detected at the receiving antenna outside the plasma. We let $t_{j,\ell}$ denote the time where the peak value of the density pulse (with label ℓ) passes through the cut-off position in the unperturbed plasma profile. The individual pulses are assumed to be integrable and to vanish for $|t| \to \infty$ but otherwise they can be chosen arbitrarily. In the following we assume the density perturbations to be pulse-like, but any other form (such as a wave-packet) can be chosen depending on the actual model for the fluctuations. With the density pulses injected randomly into the plasma and uniformly distributed in time we may write the temporally varying response in the phase signal as

$$\tilde{\phi}(t) = \sum_{\ell}^{M} \sum_{j}^{N_\ell} \phi_\ell(t - t_{j,\ell}) \tag{14}$$

where the number of pulse responses N_ℓ originating from shapes of type ℓ is itself a quantity which varies over the ensemble. With $t_{j,\ell}$ being uniformly distributed in a time record much longer than the duration of an individual response, we readily obtain (Rice, 1944) the autocorrelation function for the fluctuating phase signal

$$R(\tau) \equiv <\tilde{\phi}(t)\tilde{\phi}(t+\tau)> =$$

$$\sum_{\ell}^{M} \nu_\ell \int_{-\infty}^{\infty} \phi_\ell(t)\phi_\ell(t+\tau)dt + \left[\sum_{\ell}^{M} \nu_\ell \int_{-\infty}^{\infty} \phi_\ell(t)dt\right]^2 , \tag{15}$$

where ν_ℓ is the average number of structures of type ℓ passing the cut-off layer per unit time. Note that there is in general no logical reason for the last term to be vanishing. A power spectrum $S(\omega)$ for the phase fluctuations is defined as the Fourier transform of $R(\tau)$, and it is important to note that an arbitrary prescribed spectrum can be realized by the model (14), actually in indefinitely many ways, by the appropriate choice of ϕ_ℓ for $\ell = 1,2,...,M$.

The result (15) refers to a one-frequency reflectometer, but it is easily generalized to its two-frequency counterpart. When the density pulse passes the cut-off layer corresponding to the frequency of the *second* reflectometer it gives rise to a phase variation

$$\tilde{\psi}(t) = \sum_{\ell}^{M} \sum_{j}^{N_\ell} \psi_\ell(t - t_{j,\ell} - D/u_j) \tag{16}$$

where $u_j \neq 0$ is the velocity of the j-th pulse and D is the distance between the two cut-off layers. The time $t_{j,\ell}$ is still referring to the crossing of the *first* cut-off layer as in (14). Note that we use different notations for the two phase signals, i.e. ϕ_ℓ and ψ_ℓ will probably look rather similar, but because of the difference in local plasma density (and possibly density gradients) at the two positions they will not be *identical*. The autocorrelation function for $\tilde{\psi}(t)$ is obtained in a form quite similar to (15) while the more interesting crosscorrelation takes the form

$$R_c(\tau) \equiv <\phi(t)\psi(t+\tau)> =$$

$$\sum_{\ell}^{M} \nu_\ell \int\int_{-\infty}^{\infty} \phi_\ell(t)\psi_\ell(t+\tau - D/u)P(u)du\,dt$$

$$+ \left[\sum_{\ell}^{M} \nu_\ell \int_{-\infty}^{\infty} \phi_\ell(t)dt\right]\left[\sum_{\ell}^{M} \nu_\ell \int_{-\infty}^{\infty} \psi_\ell(t)dt\right], \qquad (17)$$

where $P(u)$ is the probability density of velocities u, which is here taken to be independent of pulse shape. For cases of interest here both polarities of density pulses are equally probable and the last, constant, term in (15) and (17) is vanishing.

As working hypothesis we first assume that $\phi_\ell(t) \approx \psi_\ell(t)$, which can actually be a good approximation when the two cut-off layers are close. With the previous definition of $S(\omega)$ we obtain the Fourier transform $S_c(\omega)$ of (17) as

$$S_c(\omega) = S(\omega)\int_{-\infty}^{\infty} e^{-i\omega D/u}P(u)du. \qquad (18)$$

For the case where all density pulses have the same velocity, i.e. $P(u) = \delta(u - u_o)$ we have the particularly simple case

$$S_c(\omega) = S(\omega)e^{-i\omega D/u_o}. \qquad (19)$$

showing that all frequency components undergo a phase change proportional to ω with a coefficient D/u_o which can be used to determine u_o. In this particular case the crosscorrelation (17) is just a shifted copy of the autocorrelation (15) and a characteristic velocity is obtained unambiguously. Here $S(\omega)$ coincides with the crossspectrum with the present assumptions. However, in the case where the difference between $\phi_\ell(t)$ and $\psi_\ell(t)$ is nontrivial, it is no longer possible to write $S_c(\omega)$ as a real spectrum with the phase variation given in the form as in (19), and a velocity of propagation is no longer uniquely defined.

In the case where the pulse velocities are statistically distributed, we have to solve (18) with the actual probability density $P(u)$ even when the approximation $\phi_\ell(t) \approx \psi_\ell(t)$ remains applicable.

We considered two examples: first a box-like distribution

$$P(u) = \begin{cases} \frac{1}{b-a} & \text{for } 0 < a < u < b \\ 0 & \text{elsewhere} \end{cases} \qquad (20)$$

The integral in (18) can then be solved analytically with the result

$$\int_a^b e^{-i\omega D/u}du = -\frac{1}{a\Omega}e^{-i(\alpha-1)\Omega} - ie^{i\Omega}E_1(a\Omega) + \frac{1}{\Omega} + ie^{i\Omega}E_1(\Omega) \qquad (21)$$

where $\alpha \equiv a/b$ and $\Omega = \omega D/a$ while $E_1(x) \equiv \int_x^\infty \frac{1}{u}e^{-iu}du$. Using (21) we can rewrite (18) in the form $F(\Omega)e^{-i\theta(\Omega)}$ with $\theta(\Omega)$ shown in Fig. 5 for two values of α. Evidently, for $\alpha = 1$ we recover the representation (19), i.e. $\theta(\Omega) = \Omega$. For $\alpha < 1$ we find that $\theta(\Omega)$ is no longer a straight line, but has a curvature, which increases with decreasing α. Another observation is that the curve deviates from the slope corresponding to that given by the average of pulse velocities, i.e. $(a+b)/2$ in the present model for $P(u)$. This line is dotted on Fig. 5.

In another model we assumed

$$P(u) = \frac{1}{\sigma\sqrt{\pi}}e^{-[(u-u_o)/\sigma]^2}. \qquad (22)$$

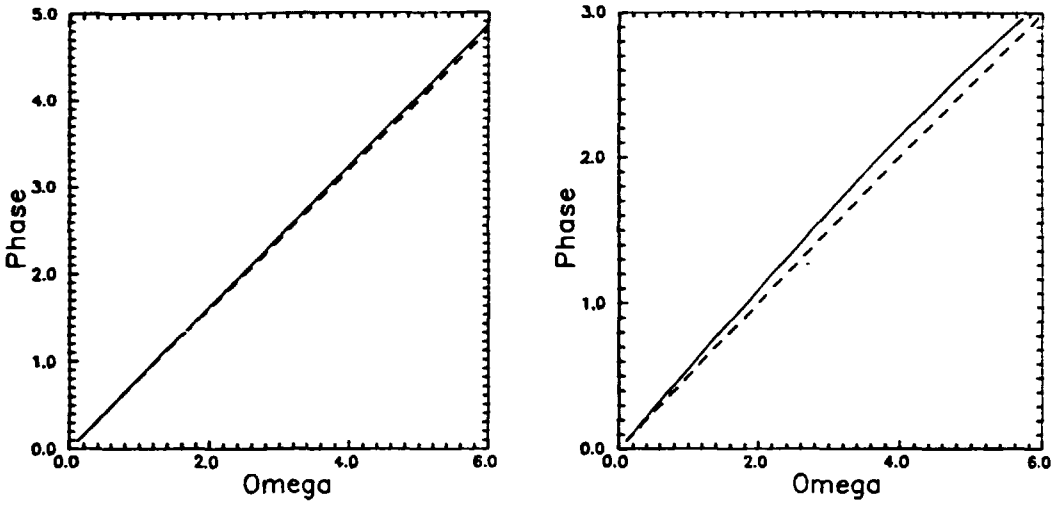

Figure 5. The function $\theta(\Omega)$ calculated for a box-like pulse velocity distribution for two values of $\alpha = a/b$, see (20) and (21). The dotted line shows the average pulse velocity. a) $\alpha = 0.67$ and b) $\alpha = 0.33$.

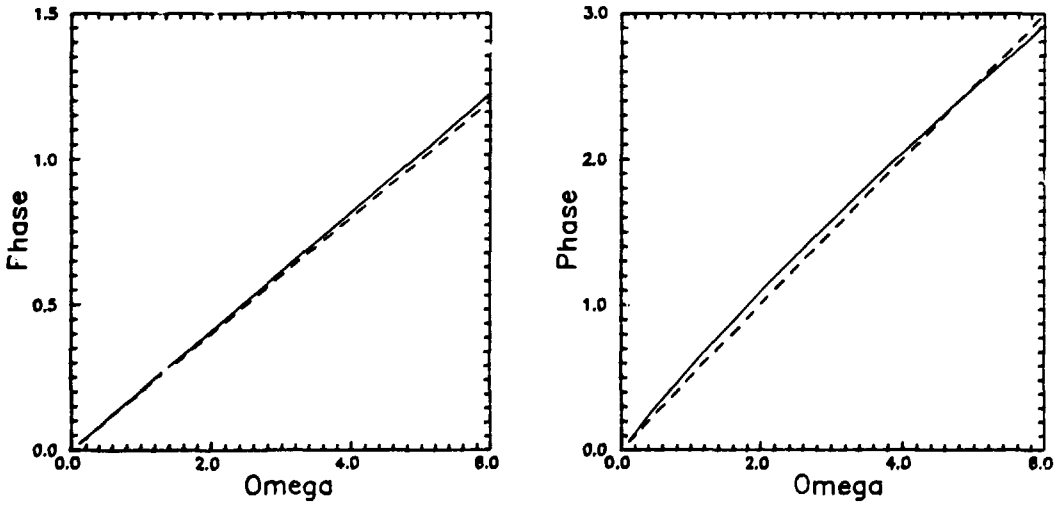

Figure 6. The function $\theta(\Omega)$ calculated for a Gaussian pulse velocity distribution for two values of α. The dotted line shows the average pulse velocity. a) $\alpha = 0.67$ and b) $\alpha = 0.33$.

The integral in (18) was evaluated numerically and the curve $\theta(\Omega)$ with $\Omega \equiv \omega/\sigma$ is shown in Fig. 6. Again, in the limit $\sigma \to 0$ we recover (19). For $\sigma > 0$ we again find that $\varphi(\Omega)$ is no longer a straight line and that its average slope can deviate from the one determined by u_o in (22), see dotted line on Fig. 6. The model (22) is used only in cases where it is safe to assume that $P(u \leq 0) \approx 0$.

We may conclude that the slope of the phase function $\theta(\Omega)$ gives a quite acceptable approximation to the average pulse velocity for narrow pulse velocity

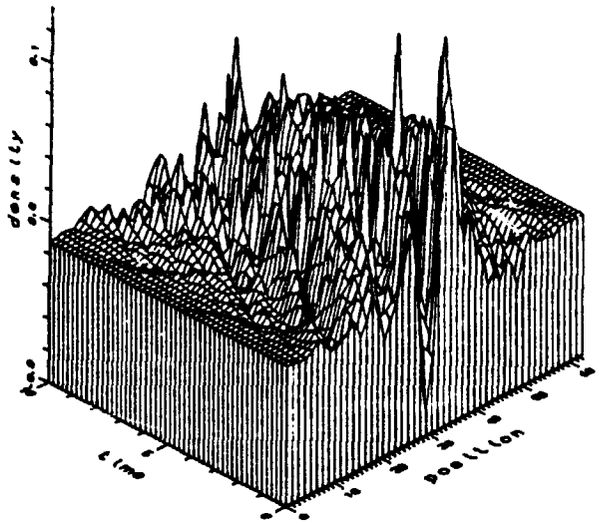

Figure 7. An example of the noise shown in a constant density plasma background. Note that we require the noise to vanish at the boundaries.

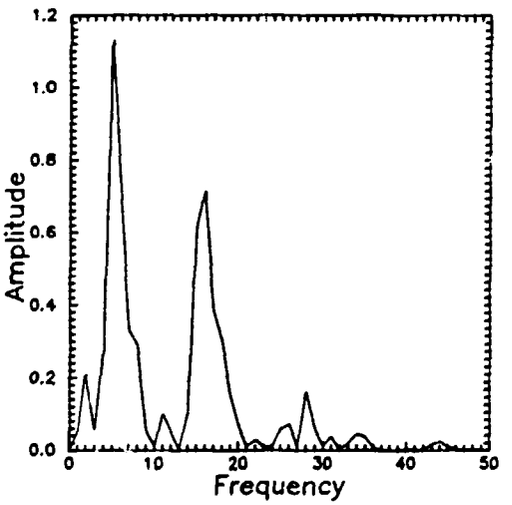

Figure 8. The frequency spectrum of the phase variation of the reflected signal obtained from the noise shown in Fig. 7.

distributions $P(u)$ in (18). This approximation deteriorates for increasing scatter of pulse velocities, and eventually the results can depend critically on the actual choice of $P(u)$.

In Fig. 7 an example of a plasma of constant density superimposed with the noise is shown. The average amplitude of the noise varies with position with a maximum of $x = 10\pi$. In Fig. 8 a spectrum of the phase variation due to this noise is shown.

Finally, we model plasma waves also by pulses of random positive or negative

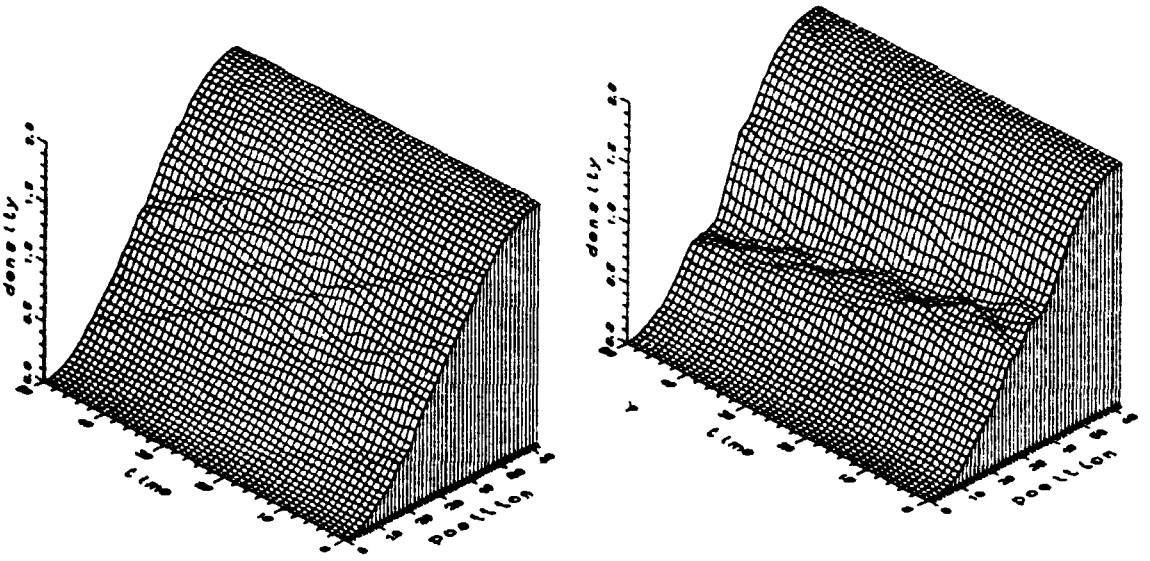

Figure 9. Density profile versus time. a) Only noise pulses are included, b). Both wave and noise pulses are included.

amplitudes, random widths, and moving with a given average velocity. The pulses each have a constant velocity which is a sum of the average velocity plus a certain random velocity specified to some limited interval. Initially the pulses are distributed randomly in space. During a run pulses disappear when they move out of the plasma, but new pulses are injected at the other boundary at random times with a given average injection rate, specified by the average number of pulses. In Fig. 9a an example of a density profile with noise pulses included is shown, and in Fig. 9b both noise pulses and wave pulses are included.

The phase of the reflected wave is calculated for each time step. Phase curves for two different reflection points i.e. two frequencies are produced for correlation analysis. An example of the phase variation with time is shown in Fig. 10. The phase variation is restricted to the interval $[-\pi;\pi]$. In practice it need not be evident how this restriction is achieved and problems may occur, which are not accounted for in the constructions (14) or (16)

In the present study we used density perturbations generated by a superposition of puls-like individual perturbations, Evidently *any* form can be used for Φ and Ψ in (14) and (16), also long wave packets and similar. It is possible to perform a quite detailed simulation of any actually observed spectrum of perturbations.

5.2 Correlation analysis

From our model calculation we get the two phase curves as discussed above. In a real experiment the amplitude of the reflected wave will be smaller than the injected wave due to geometrical expansion of the beam, the scattering due to plasma turbulence and to plasma damping. However, these processes should not have any effect of importance on the phase of the reflected wave. On the other hand it is probably very difficult to extract information about the plasma from amplitude (power) measurements. Since the phase shift depends on the variation of the plasma density between the antenna and the reflection point it is not

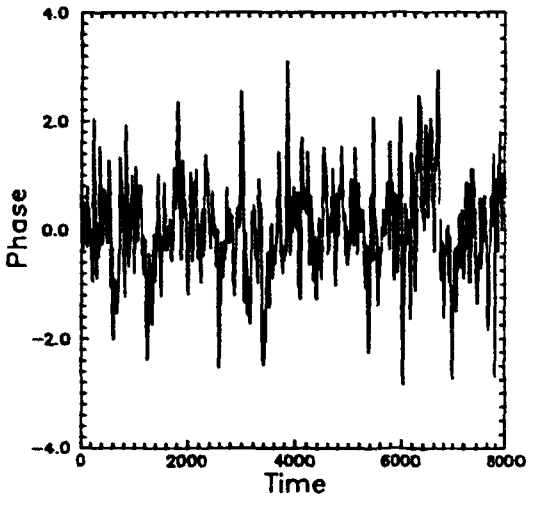

Figure 10. An example of the phase as function of time for 8192 time steps.

possible to know a priori which information can be extracted from the phase measurements. By considering a small perturbation moving along x we find a large contribution when the perturbation passes the cut-off point which decreases when the perturbation moves to lower densities. This decrease is monotonic when the perturbation length is larger than the wavelength, but oscillating when the perturbation is short compared to the wavelength (See Fig. 4). The phase change in the reflected signal will depend on the size and shape of the perturbation, and the density function in front of the cut-off layer, especially the slope of the density near the cut off-layer. If the reflection point of the two reflectometers are close, the two phase change signals should be similar and since the large contribution comes at the time when the perturbation passes the cut-off layer it should be possible by correlation techniques to determine the time of flight of the passing perturbations. If the distance between the two reflection points is determined by single reflectometry the perturbation velocity may subsequently be calculated. To investigate how well this can be done if there is a spread in perturbation velocity and there is other kind of turbulence in the plasma is the objective for the following investigation. If the phase signal exactly gives the position of the cut-off layer the problem is easy. However since this is not the case the solution to the problem is not obvious.

Let the two phase-signal be $\phi_1(t)$ and $\phi_2(t)$. Then we can calculate the correlation function:

$$R(\tau) = \frac{1}{T}\int_0^T \phi_1(t)\phi_2(t-\tau)dt \tag{23}$$

and the Fourier transform of the correlation function:

$$F(\omega) = \frac{1}{2\pi}\int_{-\infty}^{\infty} R(\tau)e^{i\omega\tau}d\tau \tag{24}$$

From a numerical point of view the Fourier transform of the correlation function can, however, be found in a more easily wave as:

$$F(\omega) = G(\phi_1(\omega))H^*(\phi_2(\omega)) \tag{25}$$

where G is the Fourier transform of ϕ_1 and H^* is the complex conjugate of the Fourier transform of ϕ_2. In this way the calculation can utilize the fast Fourier transform.

In the case where the functions $\phi_1(t)$ and $\phi_2(t)$ are only known in a discrete number of points, the correlation function and the Fourier transform has the following forms:

$$R_j = \sum_{k=0}^{N-1} g_{j+k} h_k \tag{26}$$

$$H_n = \sum_{k=0}^{N-1} h_k e^{2\pi i k n/N} \tag{27}$$

If the phase responses from a perturbation passing the cut-off layers corresponding to the two reflectometer frequencies are similar we should expect the correlation function $R(\tau)$ to be peaked, and the time shift of the peak should be the time of flight of the perturbation. From the Fourier transform $F(\omega)$ we can obtain the distribution of perturbation amplitudes and the phase shift versus frequency, and thereby the perturbation velocity.

In Fig. 11a the correlation function is shown in a case with wave pulses propagating in a plasma without any noise. All the pulses move with the same velocity. The corresponding crossamplitude spectrum is shown in Fig. 11b, and in Fig. 11c is shown the phase shift of the various Fourier components. The peak of the correlation function is, of course, shifted corresponding to the pulse velocity. However, the shift is of the order of 20 time steps and, therefore, not easily recognizable on Fig. 11a

In Fig. 12a the correlation function is shown in a case with wave pulses propagating in a plasma without any noise. All the pulses move with a velocity chosen randomly in a range of ± 0.2 times the average velocity. The corresponding cross-correlation function is shown in Fig. 12b, and in Fig. 12c is shown the phase shift of the various Fourier components.

In Fig. 13a the correlation function is shown in a case with wave pulses propagating in a plasma without any noise. All the pulses move with a velocity chosen randomly in a range of ± 0.5 times the average velocity. The corresponding crossamplitude spectrum is shown in Fig. 13b, and in Fig. 13c is shown the phase shift of the various Fourier components.

In Fig. 14a the correlation function is shown in a case with wave pulses propagating in a plasma with noise pulses included. The spread in wave pulse velocity is 0.2 times the average velocity. The corresponding crossamplitude spectrum is shown in Fig. 14b, and in Fig. 14c is shown the phase shift of the various Fourier components.

All the shown correlation functions up to now have been calculated from phase curves consisting of 8192 points (time steps). Some improvements in the correlation function can be obtained by dividing the phase curve into two or more equal parts, calculating the correlation function for each and taking the average of the results. This will reduce the uncertainty of the individual Fourier components on the expense of a reduced resolution of the spectrum caused by the reduction in individual record lengths. In fact this was done for all the results presented in the figures from (11) to (13), where the phase curve was divided into two parts. for the last two figures: Fig. 14a and b, and Fig. 14 the phase function was divided into four parts.

It is evident that the estimate on $\theta(\omega)$ becomes increasingly uncertain when the velocity-spread of the structures or pulses is increased, compare for instance Figs. 11c, 12c and 13c. The addition of small scale noise, as in Fig. 7, has a similar effect. The estimated value of $\theta(\omega)$ becomes particularly uncertain at frequencies

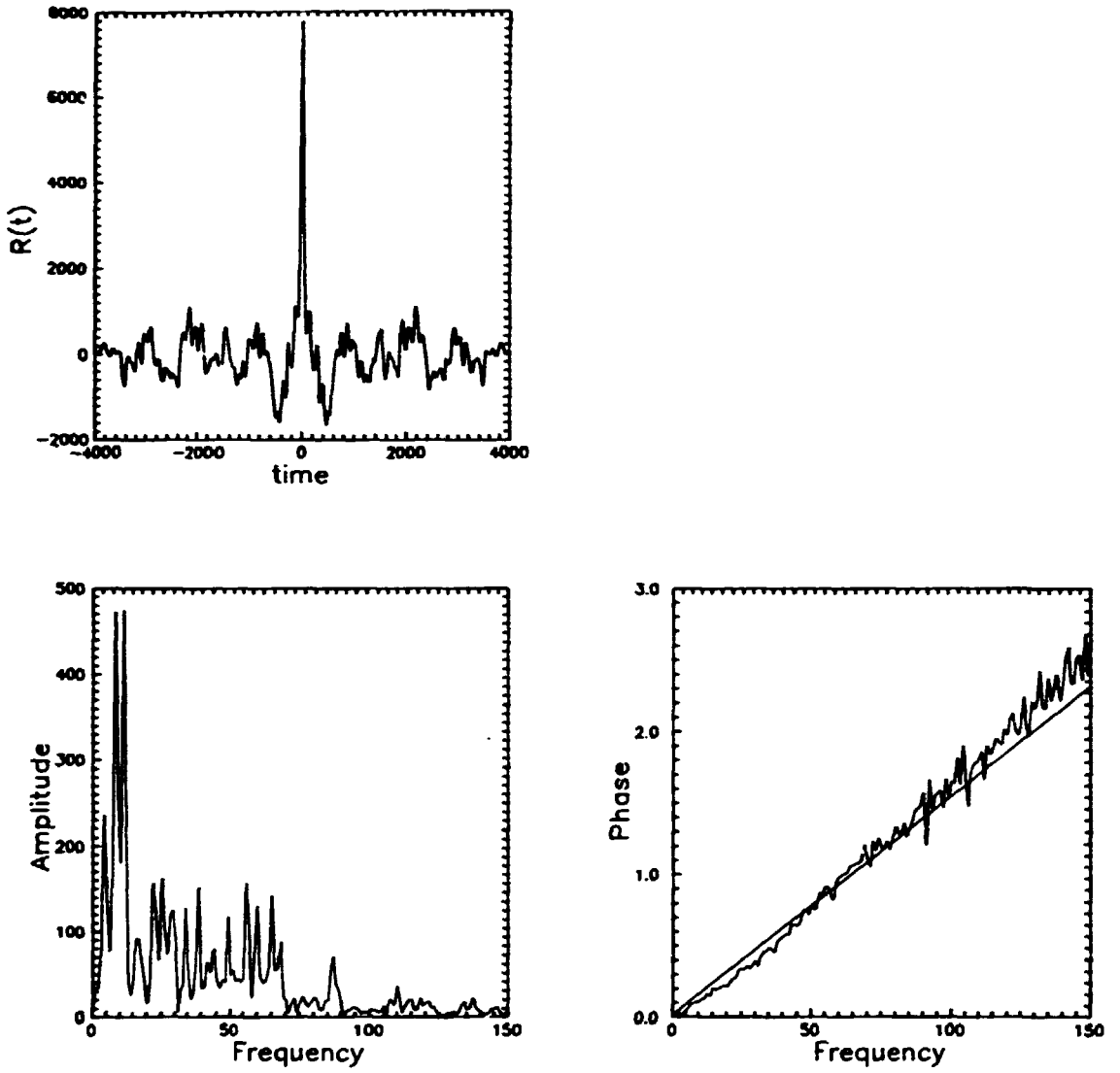

Figure 11. a) Crosscorrelation function for the two reflectometer phases in a case where many pulses are moving through a noise-free plasma, b) crossamplitude spectrum for the same case, c) velocity of the Fourier components.

where the spectral amplitude is small, since the phase is here obtained as the ratio of two small quantities. Some small gaps in e.g. Fig. 13c are caused by this effect.

6 Extremum coincidence counting

The analysis of the foregoing section demonstrated that an average pulse velocity could be estimated from the Fourier transform of the crosscorrelation for the phase fluctuations of the phase fluctuations. The resulting crosspower spectrum can be written as $S(\omega)e^{-i\theta(\omega)}$ in terms of two real quantities, a crosspower $S(\omega)$ and a phase $\theta(\omega)$, where the slope of the latter function gave a good approximation to the

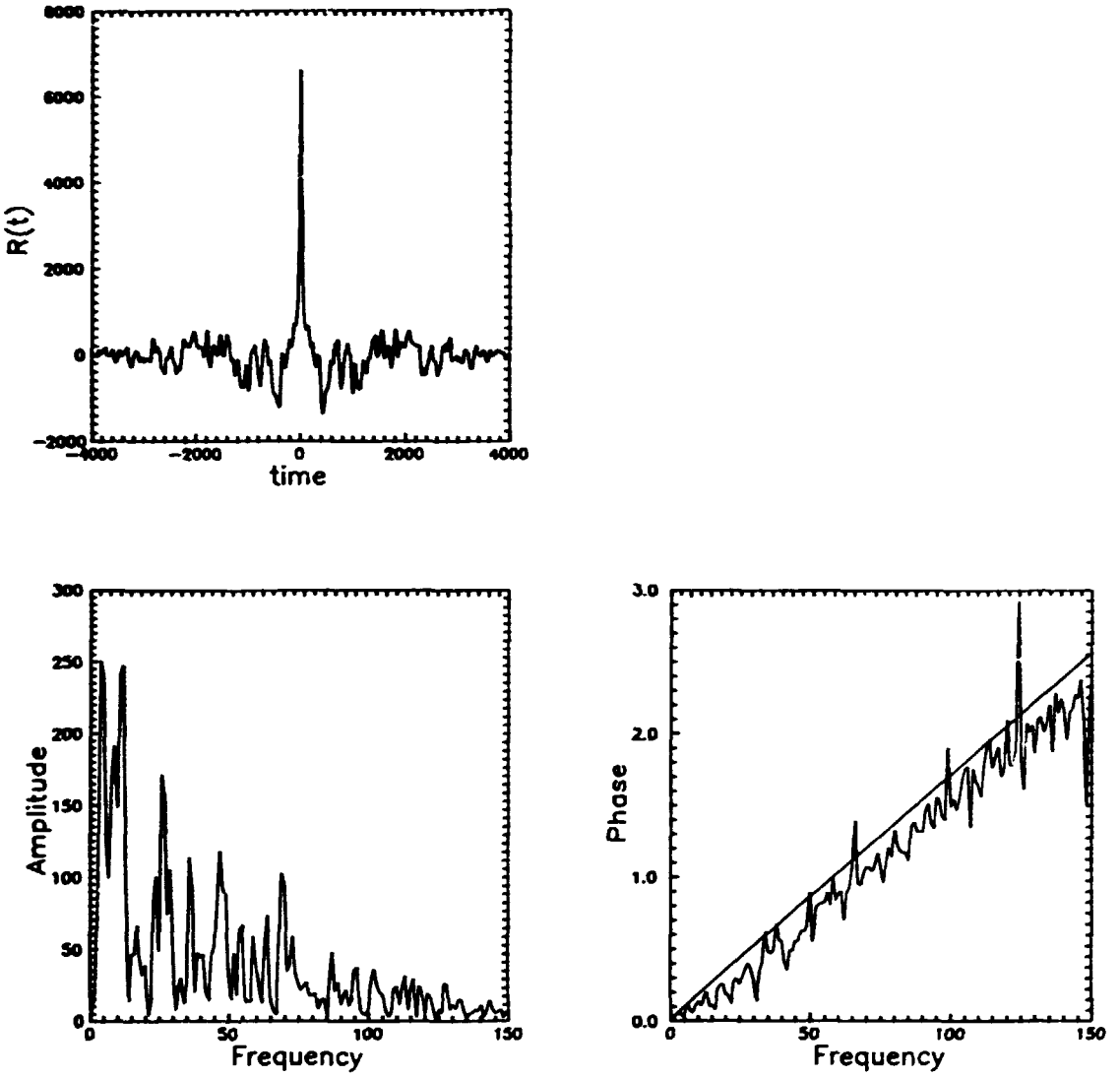

Figure 12. a) Crosscorrelation function for a case where many pulses are moving through a noise free plasma with a ±0.2 spread in velocity, b) crossamplitude spectrum for the same case, c) velocity of the Fourier components.

average pulse velocity for most practical purposes. One cannot on the basis of the phase spectrum $\theta(\omega)$ in practice distinguish the width of the velocity distribution of the propagating pulses. In this section we outline a simple alternative method, which at least for a range of parameters can distinguish between the two limits. The idea can most appropriately be termed extremum coincidence counting; every time the first record of the phase fluctuations exhibit a local maximum, the second record is searched for local maxima in a time window, which can in general extend before and after that particular reference time. (This is of course quite simple when the entire recorded is available. With analogue methods only later times are available unless a pretriggering arrangement can be devised). Local extrema are selected as reference events because they are likely to represent the time of a local extremum in deviation from the unperturbed plasma profile. This will be the case when the density of pulses is low, i.e. they are nonoverlapping. Generally there will

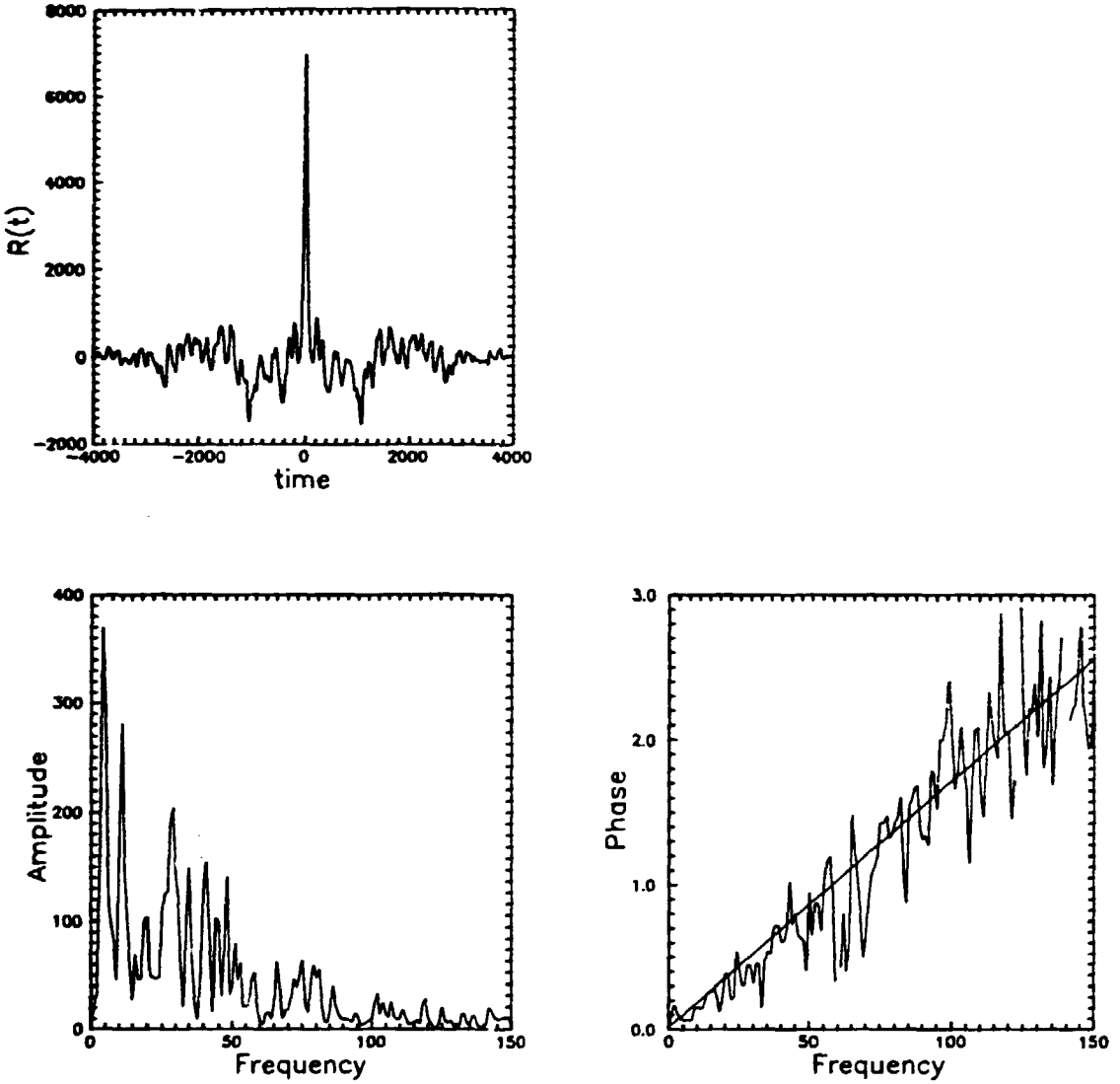

Figure 13. a) Crosscorrelation function for a case where many pulses are moving through a noise free plasma with a ±0.5 spread in velocity, b) crossamplitude spectrum for the same case, c) velocity of the Fourier components.

be a number of local extrema in record two, scattered around the reference time, t_R, where an extremum was found in record one, and most of these are entirely uncorrelated. However one particular extremum at time $t = t_R + D/u$ will be observed with large probability; this is caused by the same pulse when it passes the second cut-off layer and the two events are strongly correlated.

As an illustration we considered a case where all pulses had the same velocity and only their time of introduction into the system was chosen randomly. In Fig. 15 we show the results from a coincidence counting where local *maxima* were considered. There was no additional noise introduced in this simulation. As expected, we observe a clear peak in the countings at a time corresponding to D/U_o. Since all pulses propagate outward the peak is one-sided. The countings for *negative* times thus give the noise level, i.e. the contribution from local maxima in record two which have no relation to those in record one. Note that due to

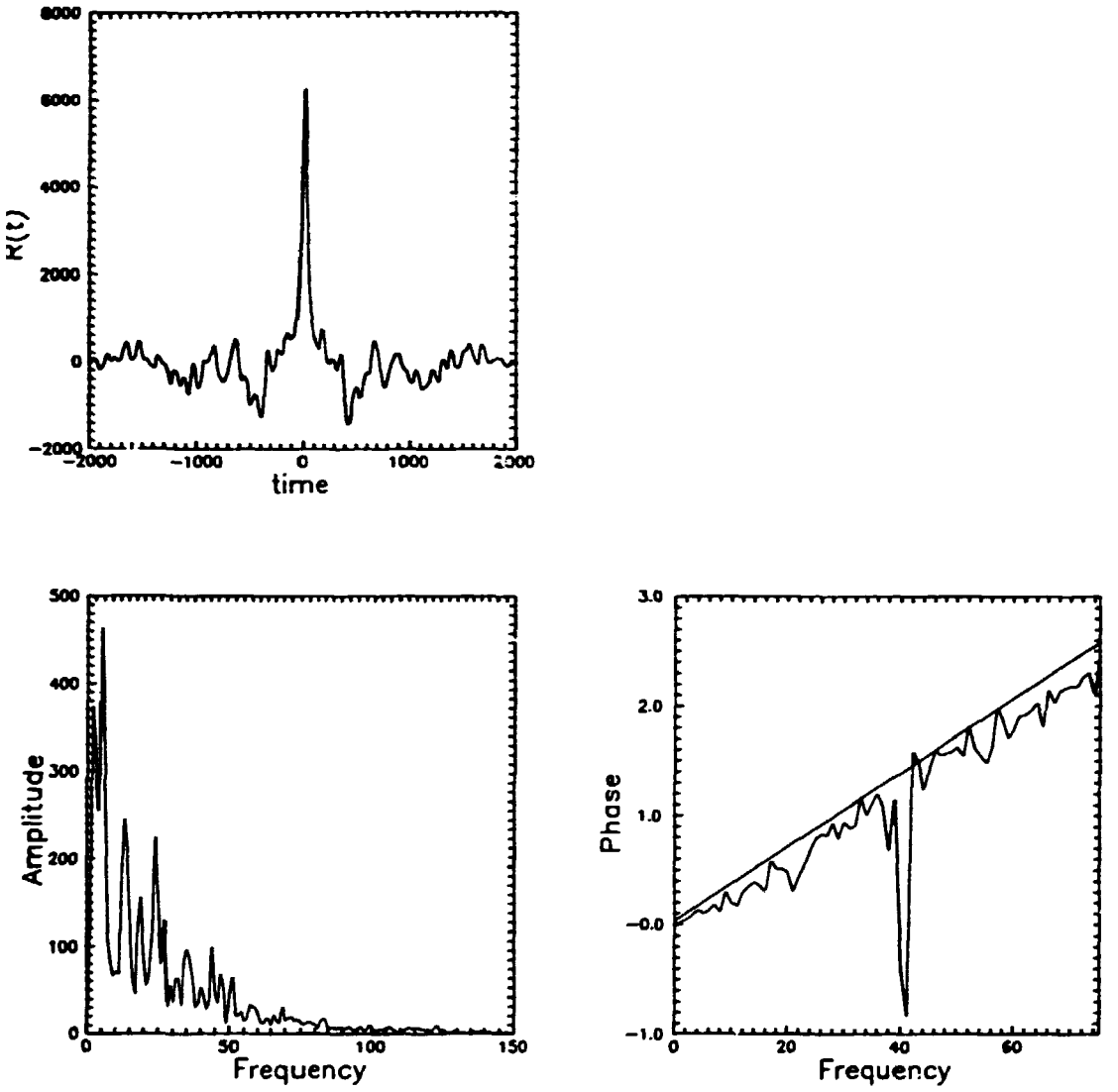

Figure 14. a) Crosscorrelation function for a case where many pulses are moving through a plasma with a noisy background, b) crossamplitude spectrum for the same case, c) velocity of the Fourier components.

the possibility of overlapping pulses, a local maximum need not coincide with the actual peak originating from an individual pulse. For reflection from narrow pulses, giving steep local density gradients, we find that one pulse gives rise to a phase "ringing", see Fig. 4, characterized by a series of local extrema. One particular feature of Fig. 15 might be emphasized; there is an apparent drop in the noise level before and after the peak at D/u_o. We argue that the local extrema of small pulses are likely to be masked if they appear on the wings of larger ones, and hence their contribution to the extrema in the phase record will be missing in the vicinity of the time D/u_o. The width of this noise-shadow region gives an estimate for the time it takes one pulse to pass through the cut-off layer. The pulse width can then be estimated since its velocity is also determined from the figure. As an additional test of this hypothesis we differentiated the phase record from the second cut off layer, and analyzed it for extremum coincidence. The results shown in Fig. 16

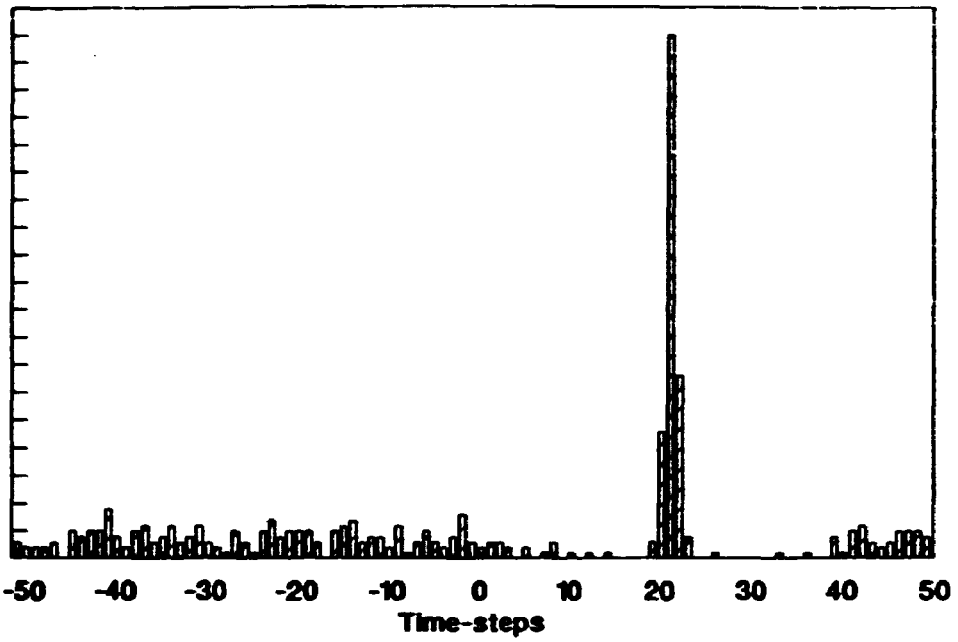

Figure 15. Coincidence counting of local maximum points of the phase curves for a case without noise and with randomly injected pulses moving with constant velocity.

clearly demonstrate an advance in time for its local maxima (i.e. points where the original record has its steepest positive gradients) and a delay for its local minima (steepest negative gradients in the original record). The time difference between the two coincidence peaks is an indicator for the pulse half-width and coincide quite well with the shadow region in Fig. 15 as expected.

In a more realistic simulation we let the pulse velocities be distributed uniformly in the interval of ±25% around the average. The results from a maximum coincidence counting is shown in Fig. 17. We note that the scatter in velocities is clearly represented in the figure, and that the standard deviation can be obtained reasonably accurately. However, the noise level is significantly enhanced, although the "shadow-effect" discussed before remains noticeable.

In a third case we added a low level noise level to the simulations, as discussed in Sec. 5.2.

The results are shown in Fig. 18 again for coincidence counting of local maxima in the two phase variations. In this case the results are entirely dominated by the reflection on the rapidly propagating noise pulses characterized by a pronounced "ringing" in the response as illustrated for one individual pulse in Fig. 4. To prove this point we repeated the calculations now using the WKB approximation, where these oscillations are absent. The results shown in Fig. 19 indeed contain only a uniform noise level with a slight peak around the origin consistent with the high velocity of the noise pulses. The individual counts come in units of 82 because of the periodicity of the noise pulses, i.e. they all have the same velocity with both directions equally probable to begin with, and a pulse leaving through one boundary is reintroduced at the other. The pulse transit time is 100 and for a total run of 8192 time steps each pulse will pass the reflection point approximately 82 times. The local peak around the average velocity of the large scale pulses is completely masked by the noise and the method thus have its clear limitations. The basic ideas are however easily implemented and certainly worth trying out

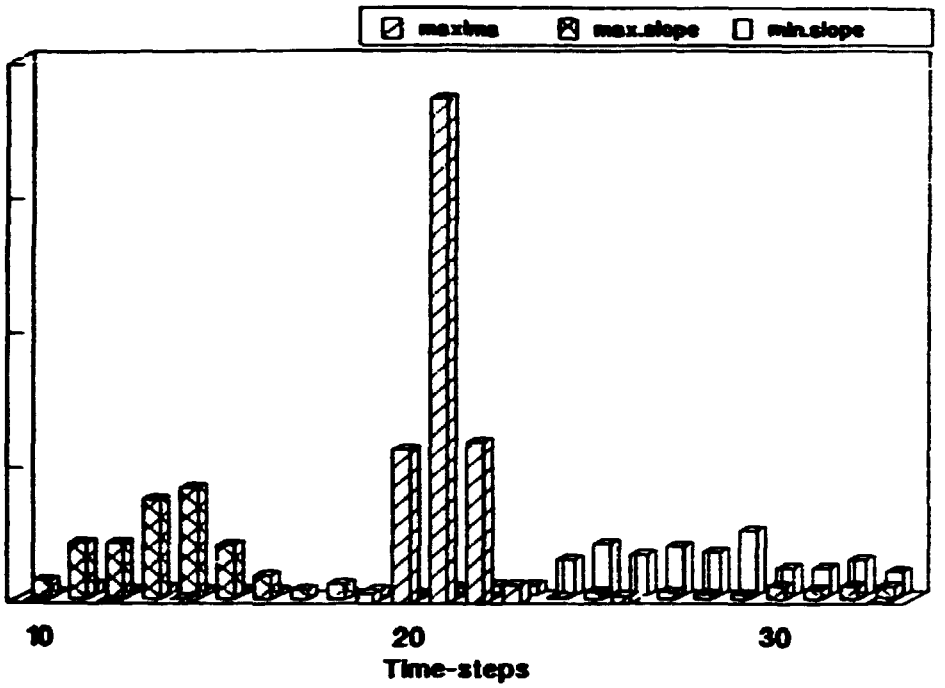

Figure 16. Coincidence counting of local maximum points of the phase curve and maximum and minimum slope for a case without noise and with randomly injected pulses moving with a constant velocity. The characteristic half-width of the pulses may be estimated as the distance between the top of the maximum slope histogram and the top of the maximum correlation histogram.

for a two beam reflectometer. The presence of a clear peak can subsequently be taken as an indication of the absence of small scale noise in the plasma.

It is plausible that a conditioned sampling of the record can give an improved signal to noise ratio. One might for instance analyze only maxima which exceed a certain level. This refinement is worth considering, but it is outside the scope of the present study.

The figures presented in this section all refer to the counting of local maxima. Evidently the same analysis can be repeated also for local minima, giving the same results since both pulse polarities have the same probability in our simulations. Taking the average of the two investigations can give a slight improvement in the signal to noise ratio.

Finally we remark that simple Monte Carlo simulations indicated that a considerable improvement of the estimation for the pulse velocity distribution can be obtained if the record from *three* sampling positions are available. This scheme would however require the extension of the reflectometer to three frequencies, and may not be practically feasible.

7 Discussion and Conclusions

In this report we studied some basic features of the performance of a two-frequency reflectometer used as a diagnostic for random plasma fluctuations. Using a realistic and tractable model for the plasma fluctuations we derived some analytical results for correlation and crosscorrelation functions for the temporally varying phase of the reflected signals. Numerical simulations were performed to illustrate

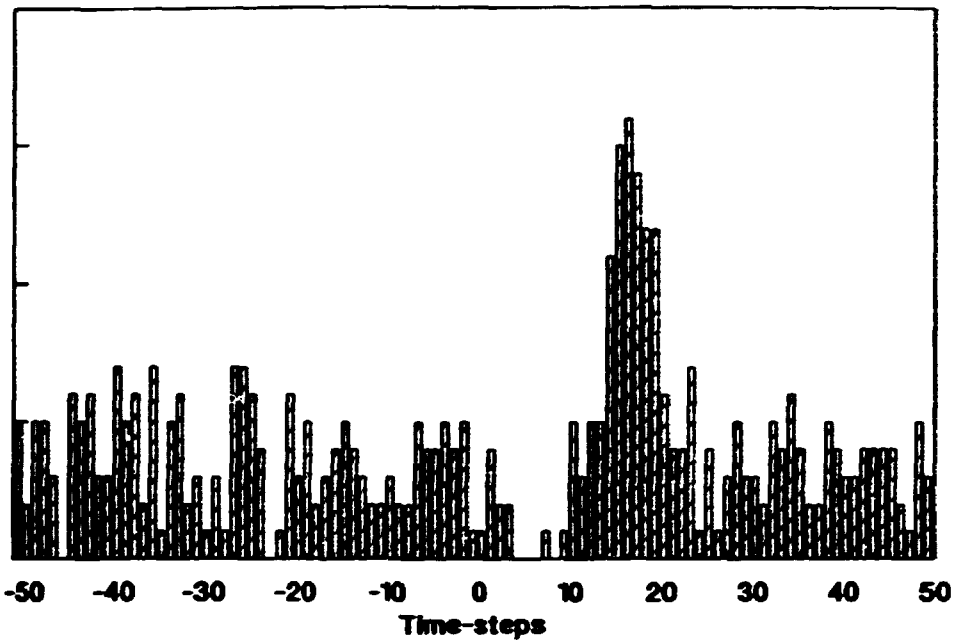

Figure 17. Coincidence counting of local maximum points of the phase curve for a case without noise but with randomly injected pulses moving with a velocity which varies ±25% around an average.

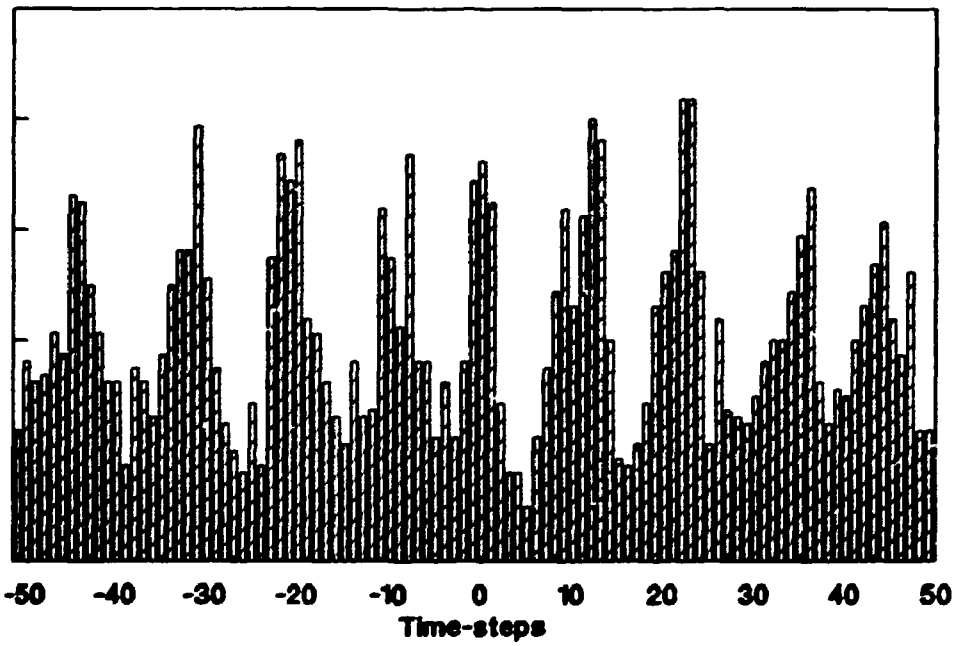

Figure 18. Coincidence counting of local maximum points of the phase curve for a case with noise and with randomly injected pulses moving with a velocity which varies ±12.5% around an average. The noise pulses introduce the periodic structure because their widths are comparable to the wavelength of the incomming wave, see Fig. 4b.

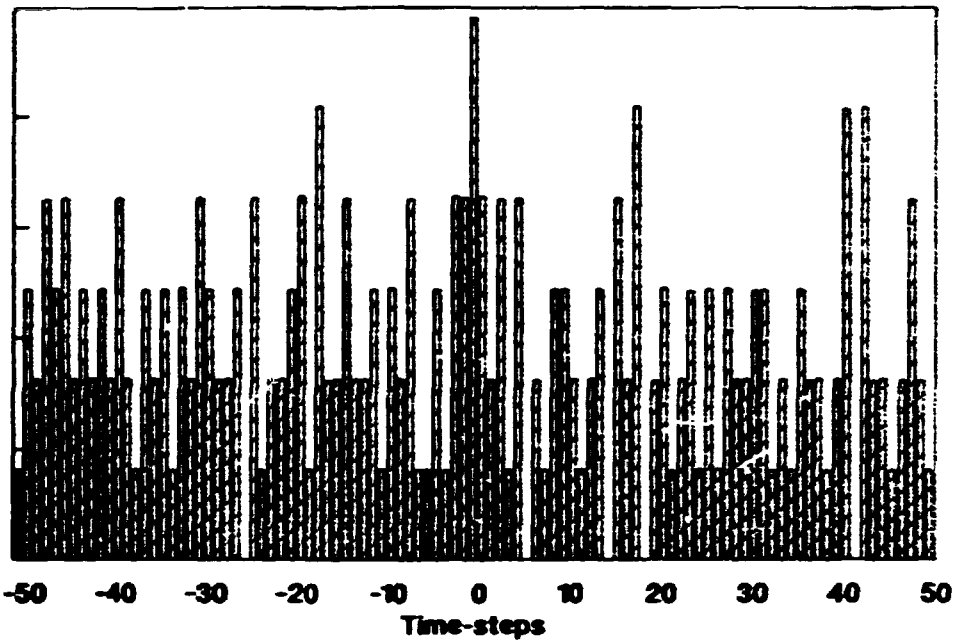

Figure 19. Coincidence counting of local maximum points of the phase curve for a case only with noise pulses but calculated assuming the WKB approximation. Note that the periodic structure seen in the figure above disappears.

the practical applicability of the basic ideas of the reflectometer. We used a simple model for the density fluctuations by letting them be composed as a random superposition of pulse-like structures. Evidently, our code allows investigation of more sophisticated models also. The studies were carried out for incoming electromagnetic waves in *ordinary* polarization, except for the results in Fig. 2 which were calculated for extraordinary polarization.

In a tokamak wave reflection can in principle occur at two different cut-off positions when the wave is launched from outside the torus. For an ordinary mode the cut-off position is where the wave frequency is equal to the plasma frequency, and for the extraordinary wave the cut-off frequency is approximately determined by:

$$\omega^2 - \omega\omega_{ce} = \omega_{pe}^2. \tag{28}$$

We assume a density profile:

$$n(r) = n_0[1 - (r/a)^2]^\alpha, \tag{29}$$

where n_0 is the maximum density, a is the minor radius of the tokamak and r is the radial position. The variation of the B-field is:

$$B = B_0 \frac{R_0}{R_0 + r}, \tag{30}$$

where R_0 is the major radius and B_0 is the B-field on the axis. If the Aspect ratio: $A = R_0/a$ and the frequency ratio $F = \omega_{pe0}/\omega_{ce0}$, where the index 0 refers to values at $r = 0$ we can write the two cut-off frequencies normalized with respect to ω_{ce0} as:

$$\Omega_O = (1 - x^2)^{\alpha/2} F \tag{31}$$

for the ordinary cut-off, and:

$$\Omega_X = \frac{1}{2(1+x/A)} + \sqrt{\frac{1}{4(1+x/A)^2} + [(1-x^2)^{-1}F^2]} \qquad (32)$$

for the extraordinary cut-off. In Fig. 20 the two cut-offs are shown versus radial position for a typical case (JET), corresponding to $\alpha = 2$, maximum density, $n_0 \approx 4 \times 10^{19} m^{-3}$, aspect ratio, $A = 2.5$, and maximum B-field, $B = 3.5T$.

Evidently our numerical studies could have been carried out just as easily for the extraordinary polarization (see Fig. 2 for a wave solution for this polarization of the incoming wave). The analysis of Sec. 5.1 did not require any specific polarization.

In applications of two-frequency reflectometers it is crucial that the frequency *difference* between the two probing waves is relatively constant. The absolute value of the frequency might on the other hand, at least for gentle plasma density gradient, vary on a slow time scale compared to the transit time of the density perturbations. There is in principle a very simple solution to this problem, i.e. the *same* generator is used for both channels of the reflectometer using one in ordinary, the other in extraordinary polarization. The two cut-off layers will for certain plasma parameter ranges be located at two nearby positions allowing investigations of the correlation of density fluctuations in the two positions. Unfortunately this plasma parameter range is uninteresting for JET and most of the large fusion experiments, as Fig. 20 shows. It is seen here that no matter which extraordinary cut-off frequency is selected, then a wave with the same frequency in *ordinary* polarization will simply propagate through the plasma and be reflected at the inner wall. Although the previously outlined scheme may be interesting for smaller devices with relatively weaker magnetic field, it is evidently unsuited for relevant JET parameters, and here it seems necessary to operate with two different frequency generators, which have to be stabilized or synchronized.

The present study have assumed the density perturbations as a priori given, without discussing the actual nature of these fluctuations. In the report of Costley and Cripwell (1989) an interpretation in terms of drift waves was advocated. However, this particular wavetype propagates predominantly in the direction per-

Figure 20. Normalized cut-off frequencies for ordinary and extraordinary mode in a typical tokamak case as a function of radial position. $\alpha = 2$, $A = 2.5$, and $F = 0.58$.

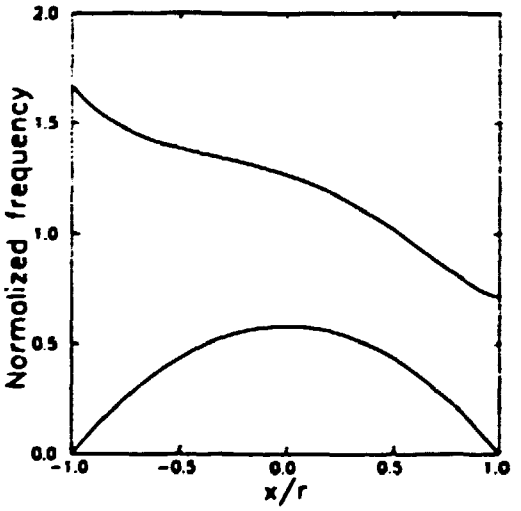

pendicular to both the local magnetic field B, and the density gradient $\nabla n_o(\mathbf{r})$, with small modifications induced by magnetic shear. A significant radial propagation velocity is most likely to be found for acoustic type fluctuations where our model is directly applicable or cyclotron waves, which however will have a significant dispersion of individual pulses.

Since Alfvén waves are incompressible, it might be expected that they should not be observable by reflectometer techniques. However, if these waves are propagating in a plasma density gradient, they may still give rise to local fluctuations in density, when the local plasma velocity associated with the wave moves plasma in and out along the gradient.

Due to limitations in the COLSYS code, the present studies were carried out in one spatial dimension. In the limit where the WKB approximation is applicable it is actually possible to carry out the numerical simulations in a fully three dimensional toroidal model using codes applied for different problems by Hansen et al. (1988b, 1988c) or Bindslev and Hansen (1991).

In summary we may state that our results indicate that a two-frequency reflectometer can in a number of cases prove to be a most versatile method for diagnosing local density fluctuations in fusion related plasma experiments. When the density perturbation have a velocity component in the direction defined by the probing electromagnetic wave beams, then this velocity component can be determined relatively accurately by a crosscorrelation of the modulated phase of the reflected waves, where the modulation is caused mainly by density perturbations propagating through the reflection point (i.e. cut-off layer) for the two waves. The studies by Costley and Cripwell (1989) were concerned primarily with density perturbation propagating in the radial direction of the plasma i.e. they used normally incident probing waves, although also other angles of incidence could be used.

The correlation technique gives results in terms of averaged velocities. We demonstrated that a relatively simple method, extremum coincidence counting, can in a number of nontrivial cases give valuable additional information. The actual *interpretation* of the results obtained by the methods discussed here is a quite different question, and will require a detailed understanding of the physical mechanisms involved in the generation of the density fluctuations.

Acknowledgements

The authors wish to thank Jens-Peter Lynov for his helpfulnes with the program package COLSYS.

References

Ascher, U., Christiansen, J. and Russell, R.D. (1979). Math. Comp. **33**, 659.

Bindslev, H. and Hansen, F.R., (1991) JET-IR (91)02.

Cavallo, A. and Cano, R. (1982). Report EUR-CEA-FC 1137.

Costley, A.E. and Cripwell, P. (1989). JET-P(89) Report 82.

Cripwell, P. and Costley, A.E. (1991). Proc. of the 18th Conf. on Controlled Fusion and Plasma Physics, Berlin, 3-7 June 1991, **15CI** 17.

Doyle, E.J., Lehecka, T., Luhmann, N.C., Peebles, W.A., and Philipona, R. (1990). Rev. Sci. Inst. **61**, 3016.

Ginzburg, V.L. *The Propagation of Electromagnetic Waves in Plasmas.* (Pergamon Press 1964.)

Hansen, F.R., Lynov, J.P., Maroli, C. and Petrillo, V. (1988a). J. Plasma Physics **39**, 319.

Hansen, F.R., Lynov, J.P., Michelsen, P. and Pécseli, H.L., (1988b). Nucl. Fusion **28**, 769.

Hansen, F.R., Lynov, J.P., Michelsen, P. and Pécseli, H.L., (1988b). Risø-M-2747.

Rice, S.O. (1944). Bell System Techn. J. **23** and **24**. reprinted by N.Wax (ed.) *Selected papers on Noise and Stochastic Processes* (Dover, New York, 1954) p. 133.

Simonet, F. (1985). Rev. Sci. Inst. **56**, 664.

Sips, A.C.C. (1991). Rijnhuizen Report 91-299.

Zou, X.L., Laurent, L., Rax, J.M. (1991). Plasma Phys. Contr. Fusion **33**, 903.

Bibliographic Data Sheet **Risø–R–592(EN)**

Title and author(s)

A Numerical Study of Reflectometer Performance

Poul Michelsen and Hans Pécseli

ISBN	ISSN
87-550-1748-7	0106-2840

Dept. or group	Date
Optics and Fluid Dynamics	December 1991

Groups own reg. number(s)	Project/contract No.

Pages	Tables	Illustrations	References
29	0	20	14

Abstract (Max. 2000 char.)

In this report some basic features of the performance of a two frequency reflectometer used as a diagnostic for random plasma fluctuations are studied. Using a realistic and tractable model for the plasma fluctuations we derived some analytical results for correlation and crosscorrelation functions for the temporally varying phase of the reflected signals. Numerical simulations were performed to illustrate the practical applicability of the basic ideas of the reflectometer. The studies were carried out mainly for incoming electromagnetic waves in ordinary polarization.

Descriptors INIS/EDB

BOUNDARY CONDITIONS; C CODES; COMPUTERIZED SIMULATION; CORRELATION FUNCTIONS; EXPERIMENTAL DATA; FLUCTUATIONS; JET TOKAMAK; PERFORMANCE; PLASMA DIAGNOSTICS; PLASMA DENSITY; POLARIZATION; WAVE EQUATIONS; WKB APPROXIMATION;

Available on request from:
Risø Library, Risø National Laboratory (Risø Bibliotek, Forskningscenter Risø)
P.O. Box 49, DK-4000 Roskilde, Denmark
Phone (+45) 42 37 12 12, ext. 2268/2269 · Telex 43 116 · Telefax (+45) 46 75 56 27

Available on request from:
Risø Library
Risø National Laboratory,
P.O. Box 49, DK-4000 Roskilde, Denmark
Phone +45 42 37 12 12, ext. 2268/2269
Telex 43116, Telefax +45 46 75 56 27

ISBN 87-550-1748-7
ISSN 0106-2840